Advanced Robotics

ISSN: 0169-1864 (Print) 1568-5535 (Online) Journal homepage: http://www.tandfonline.com/loi/tadr20

Realization of dynamic walking for the humanoid robot platform KHR-1

Jung-Hoon Kim & Jun-Ho Oh

To cite this article: Jung-Hoon Kim & Jun-Ho Oh (2004) Realization of dynamic walking for the humanoid robot platform KHR-1, Advanced Robotics, 18:7, 749-768, DOI: 10.1163/1568553041719500

To link to this article: https://doi.org/10.1163/1568553041719500

Published online: 02 Apr 2012.

Advanced Robotics, Vol. 18, No. 7, pp. 749–768 (2004)

Also available online - www.vsppub.com

Full paper

Realization of dynamic walking for the humanoid robot platform KHR-1

JUNG-HOON KIM and JUN-HO OH *

Machine Control Laboratory, Department of Mechanical Engineering, Korea Advanced Institute of Science and Technology, 373-1 Guseong-dong, Yuseong-gu, Daejeon 305-701, South Korea

Received 15 August 2003; accepted 2 December 2003

Abstract—This paper presents three online controllers for maintaining dynamic stability of a humanoid robot and describes simplified walking patterns for easy tuning in real experiments. The legs of a humanoid robot are relatively long and serially connected with compliant force/torque sensor at the ankle. This architecture has the inherent characteristics of a lightly damped system. Most research on balance control overlook the deterministic vibration caused by structural compliance. In addition, the vibration was not positively considered to improve the characteristics of the system. Therefore, a simple inverted pendulum model with a complaint joint is proposed. The proposed model has an advantage in easy parameter identification by experiment. For this model, the damping controller that increases system damping is proposed as a balance controller. Furthermore, the performance of maintaining balance against external forces is experimentally shown. A landing orientation controller at the ankle joints is presented to manage fast and stable ground contact. A landing position controller is implemented in order to modify the prescribed trajectory of the swing foot and to reduce the landing impact during unexpected landing. The effectiveness of the proposed controllers is confirmed by walking experiments that have been applied on the KAIST humanoid robot platform KHR-1.

Keywords: Biped humanoid robot; dynamic walk; balance control; damping control; inverted pendulum.

1. INTRODUCTION

Biped robots have good mobility in various environments such as rough terrain and stairs. Mobility is very important in the sense that future service robots should help and cooperate with humans in all environments. The demand for developing control algorithms of biped locomotion is increasing, but it is not a simple problem. The biped robot is unstable, nonlinear and dynamically time variant. In addition, the

*To whom correspondence should be addressed. E-mail: junhoh@ohzlab.kaist.ac.kr

biped robot needs to interact with complex environments. Biped walking is made up of the periodic phase changes between single support and double support. From the viewpoint of system response in one phase, we can say that there is no steady state and only a transient state exists. Moreover, the initial condition changes in every transition. Because of the complex nature of dynamic walking, it is meaningful to actually implement the control algorithm experimentally on the robot rather than by simulation alone. Thus, we developed the humanoid robot platform KHR-1 as a platform for the realization of dynamic walking.

Recently, research on humanoid robots has been increasing since the successful results of Honda R&D, Waseda University and Tokyo University [1–4]. In many cases, strategies for walking motion control can be classified into the walking pattern generation [4–8] related to the motion planning and online balance control [1, 9–14]. A walking pattern is generated to ensure that the zero moment point (ZMP) of the robot is inside the supporting foot at all times. This is necessary for the robot to maintain dynamic stability during bipedal walking [15]. However, the desired ZMP of the walking pattern is different from the actual ZMP of the biped robot during actual walking. In order to compensate for the ZMP error, it is necessary to implement the balance control using a force/torque (F/T) sensor or inclination sensor. Several methods of online balance control have been proposed. Some research groups realized successful dynamic walking experimentally with their own balance control scheme [1, 8, 11, 12, 14]. Kajita *et al.* introduced a balancing control using direct feedback control of the total angular momentum and the position of the center of gravity [13]. Kagami *et al.* developed AutoBalancer [14], which modifies the original input trajectories based on many criteria of stability, but Sugihara *et al.* commented that it was difficult to apply for the fast dynamic motions because of the complexity of the algorithm and the criteria themselves [16]. Huang *et al.* focused on the generation of a smooth walking pattern and their real-time modification contains a somewhat rough control equation without a mathematical model [17]. Other researchers proposed other balancing methods by simulation to improve the computation time and performance [16, 18]. Most research on balance control concentrates on the compensation of the ZMP error because the ZMP is the criteria for dynamic stability. In many cases, it has been assumed that the main cause of the error arises from the unexpected ground inclination or model inaccuracy. It is a matter of course that the balance controller should be robust for the inclination and the inaccuracy. However, by observing the experimental results of the position control during the single support phase, we noticed that the compliance near the ankle joint mainly introduced the ZMP error. The compliance results from the relatively long leg that is serially connected with a compliant F/T sensor at the ankle. In most research, the deterministic vibration has been overlooked in the balance control and was not positively considered to improve the characteristics of a lightly damped structure.

In this paper, we propose a simple inverted pendulum model with a compliant joint during the single support phase, and design a damping controller as a balance

controller that improves the damping capability of the system. Its performance of damping out the inherent vibration is experimentally shown. In addition to this, we present the landing orientation controller that makes a smooth and fast touchdown of the swinging leg without resistance. The damping controller and the landing orientation controller are alternated between every phase transition. A landing position controller is also implemented because the unexpected touchdown needs modification of the foot position in the vertical and horizontal directions. The modification are such that the moment between the two feet and the impact force are altered to maintain the stability of the robot. Consequently, stable walking could be realized by experiment with these three controllers.

2. HUMANOID ROBOT PLATFORM DESCRIPTION

2.1. Mechanical structure

The KHR-1 is shown in Fig. 1. Its total weight, including batteries, computer, controllers and amplifiers, is 48 kg and its height is about 120 cm. The KHR-1 has 21 d.o.f. Each leg has 6 d.o.f. and it can imitate human walking motion in the sagittal and the frontal plane. The dimension and the d.o.f. of KHR-1 are shown in Table 1. The KHR-1 was designed to have a kinematically simple structure. A complicated mechanical design such as a differential mechanism was avoided. Harmonic drive gears were used as the main reduction gears. A pulley-belt and bevel gears were also used for transmission. The actuators of the lower limbs were selected by the simulation of specific motion patterns in the sagittal and lateral plane

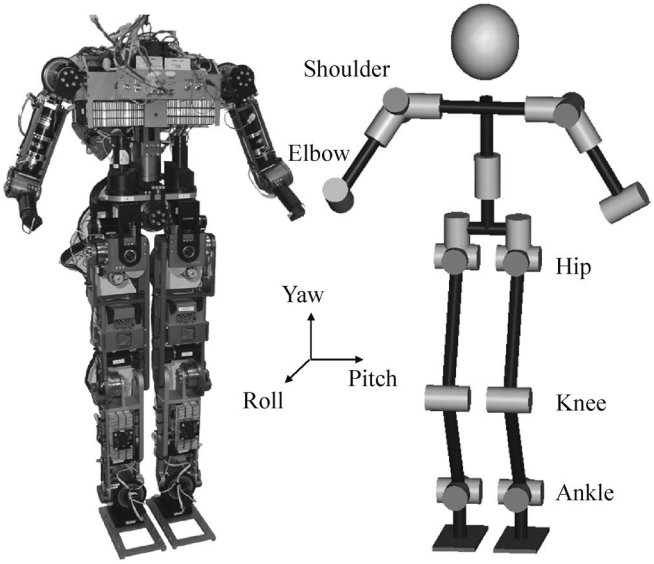

Figure 1. Photograph and joint structure of KHR-1.

with a simple lumped mass model [19, 20]. For example, a specific motion pattern in sagittal plane is a standing up and sitting down motion during the single support phase, and this pattern is frequently observed in walking and going up stairs. Based on the simulation results, appropriate motor specifications and reduction ratios were selected as shown in Table 2. Because a high load is not applied in the yaw axis

Table 1.
Specification of the humanoid robot

Weight (kg)		48 kg
Dimensions (mm)	height (without head)	1193 mm
	width	484 mm
	depth	230 mm
	length of upper arm	255 mm
	length of upper leg	340 mm
	length of lower leg	305 mm
d.o.f.	arms	shoulder 3×2
		elbow 1×2
	waist	1 (yaw)
	legs	hip 3×2
		knee 1×2
		ankle 2×2
	total :	21

Table 2.
Gear ratio and motor power of each joint

			Gear ratio of harmonic drive ([] = transmission ratio)	DC motor power (W)
Arm	shoulder	Y	100 : 1	20
		R	100 : 1	90
		P	100 : 1	20
	elbow	P	100 : 1	90
			[2 : 1] bevel gears	
Trunk		Y	100 : 1	90
Leg	hip	Y	100 : 1	90
		R	120 : 1	150
			[35 : 12] pulleys	
		P	120 : 1	150
			[35 : 12] pulleys	
	knee	P	160 : 1	150
			[1.5 : 1] pulleys	
	ankle	R	100 : 1	90
			[13 : 7] pulleys	
		P	100 : 1	90
			[2 : 1] pulleys	

of the hip joint, a 20 W motor is sufficient in this joint. However, a 90 W motor was used since there was little difference in size and weight. Contrary to the lower limbs, the design objective of the upper body was more focused on the lightweight and compact structure rather than the power analysis.

2.2. Hardware architecture

Figure 2 shows the overall block diagram of the robot controller. A Pentium III-500 embedded computer with a PC104 interface is used as a master controller. It interfaces with two peripheral interface boards (PIB) that can control 12 DC motors. The PIB is equipped with 12 PWM generators and encoder counters built with a Programmable Logic Device (PLD). The master controller generates joint position commands at 100 Hz by sensor feedback and a linear interpolation of digital PD controllers for the DC servomotor is running in the background at 1 kHz in a DOS environment.

In controlling the multi-axis system simultaneously, it is effective to use a decentralized control, where the main controller communicates with each subcontroller module which controls joint motors. To create an internal network, serial bus connections using RS-485 or Controller Area Network (CAN) are often used. However, a central control scheme is used in this system, where the main computer controls all the servomotors directly. Since it is easy to modify the program for an entire submodule by editing a library file, this method has its own advantage in the development stage in which lots of tests are done.

The PIB also has a built-in microcontroller (PIC16F876) that receives the measured force and torque data *via* RS-232 communication from the F/T sensor attached to the sole of the robot. This microcontroller communicates with the main computer *via* a parallel interface implemented by an 8255 chip. The force and torque data are updated at 100 Hz. An eight-channel A/D converter is used to read analog signals from additional sensors such as rate gyro and accelerometer, etc.

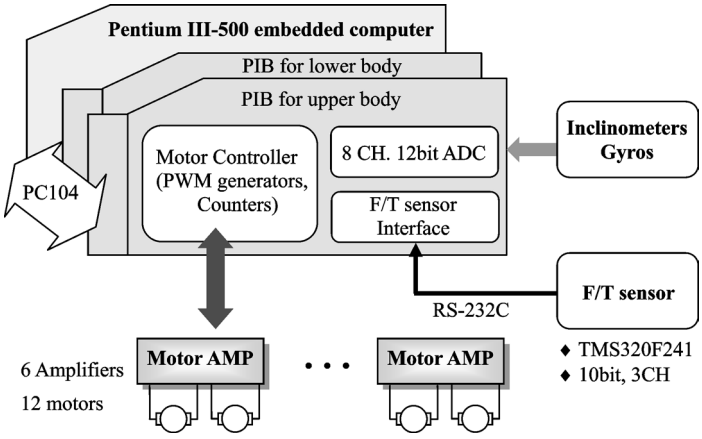

Figure 2. Hardware architecture.

2.3. F/T sensor

The sensors that are generally used in a humanoid robot are categorized by their level in Table 3. The fundamental first sensor level is the kinesthesia such as the current that is generated in each joint motor and the F/T information at the ankle or wrist. The second sensor level corresponds to the vestibular organ of a human that senses the equilibrium of the body. Accelerometers, inclinometers and rate gyros belong to this second level. The stabilization of walking is possible with the first-level sensor (F/T sensor) on the flat ground. The second-level sensors will improve its performance when disturbances occur. The third-level sensors are the vision sensor, which is related to space perception, and the tactile sensor. These sensors enable highly advanced recognition and expand the ability of interaction with humans. In this study, we will focus on sensory feedback using only a F/T sensor. After maximizing the performance with minimum sensors, we will improve the performance with additional sensors in the future research.

It is necessary to measure the F/T of the foot in order to calculate the actual ZMP. We developed the F/T sensor that can measure two moments up to 34 Nm along the roll and pitch axes, and one normal force up to 950 N in the vertical direction. It consists of three strain gage bridges to measure two moments and one force. Each strain gage bridge is composed of four strain gages attached to the mechanical structure of sensor. We chose an appropriate location of the strain gage so that a cross-coupling signal should be eliminated. That is, applied force or torque activates only the corresponding bridge circuit without generating a cross-coupling signal to the other circuit. The structure is made of duralumin. Due to the compact size (80 mm $\times$ 80 mm $\times$ 25 mm) and light weight (200 g), it can easily be mounted to the sole of a foot. The electronic circuit of the F/T sensor has a built-in microcontroller (TMS320F241) which controls a multiplexer and programmable gain amplifier; 150 times gain is used for moment, while 860 times gain is used for force. The on-board microcontroller is capable of eliminating the output offset under unstrained conditions. It transmits the measured signal to the master controller *via* RS-232 communication or CAN at 100 Hz.

Table 3.
Sensor level that is used in the humanoid robot

Level	Sensory organ	Sensor
1	muscle, tendon	F/T sensors at the ankle and wrists
	(kinesthesia)	current sensors for each motor
2	vestibular organ	accelerometers/inclinometers
	(sense of equilibrium)	rate gyros
3	eye	vision system
	(space perception)	tactile sensors
	tactile organ	etc.

3. DAMPING CONTROLLER AT THE ANKLE JOINT

3.1. Simple inverted pendulum model with a compliant joint

As a model of bipedal walking during the single support phase, the inverted pendulum model, flywheel model and acrobat model can be assumed [21]. The link is generally assumed to be rigid in many cases, but in a real situation it is flexible because the foot is connected with a compliant F/T sensor and the leg length is relatively long compared to its cross-section. Due to this compliance, the humanoid robot exhibits the characteristics of a lightly damped structure. For example, during the single support phase when the ankle is under position control, the external force will easily excite a sustained oscillation. The oscillation exists even when the position error is nearly zero. When this inherent oscillation occurs, position control of biped walking cannot succeed even if the exact trajectory that satisfies the desired reference ZMP is known. This phenomenon is even prevalent in the fast gait. Therefore, it is desirable to perform the position control considering the stiffness of links using torque feedback. In this paper, a single mass inverted pendulum with a compliant joint is considered as the suitable model as shown in Fig. 3 where u denotes the ankle joint angle and θ denotes the actual inclined angle produced by the compliance. The output y is the torque T from the F/T sensor. From the model shown in Fig. 3, the equation of motion is derived as:

$$y = T = mgl\theta - ml^2\ddot{\theta}, \tag{1}$$

$$T = K(\theta - u). \tag{2}$$

The transfer function from the ankle joint angle to the torque is derived from the above two equations [22]:

$$\frac{y}{u} = \frac{T}{u} = K\frac{-s^2 + \dfrac{g}{l}}{s^2 + \left(\dfrac{K}{ml^2} - \dfrac{g}{l}\right)} = K\frac{-s^2 + (\beta - \alpha)}{s^2 + \alpha}, \tag{3}$$

where

$$\alpha = \frac{K}{ml^2} - \frac{g}{l} > 0, \quad \beta = \frac{K}{ml^2},$$

K is the stiffness of the leg, g is gravity, l is the length of pendulum and m is the mass, respectively.

If the damping coefficient C of the link is considered, the torque in (2) can be expressed as $T = K(u - \theta) + C(\dot{u} - \dot{\theta})$. However, for simplicity, the damping coefficient is neglected in this paper, since its value is relatively small compared to the stiffness.

The ankle joint angle u is generated by the reference command u_{ref} in the PD position feedback configuration shown in Fig. 4. The transfer function T/u_{ref} in Fig. 4 has similar dominant poles and zeros with T/u of (3), and also has negligible

fast poles over 600 rad/s which correspond to the motor dynamics. Thus, it is valid to regard u_{ref} as u. So, the transfer function can be approximated by the following equation:

$$\frac{T}{u_{\text{ref}}} \simeq \frac{T}{u} = K\frac{-s^2 + (\beta - \alpha)}{s^2 + \alpha}. \tag{4}$$

It is also valid to design a feedback controller for (4) if the closed loop pole is assigned near to the dominant system poles. As shown in (4), the pole is near the imaginary axis of the s-domain and the system is a non-minimum phase plant. The parameters of (4) can be found by experimental identification. By measuring the oscillation period under position regulation control during the single support phase, we can calculate α. By measuring the torque increment for ankle angle increment at steady state, we can also get $K(\beta - \alpha)/\alpha$. From the two equations, l and K can be identified. In addition, measuring a sinusoidal response for various input frequencies is another method for verification. When the model is very complicated, it is actually hard to identify all the parameters. However, the proposed model has an advantage in simple and easy parameter identification by experiment.

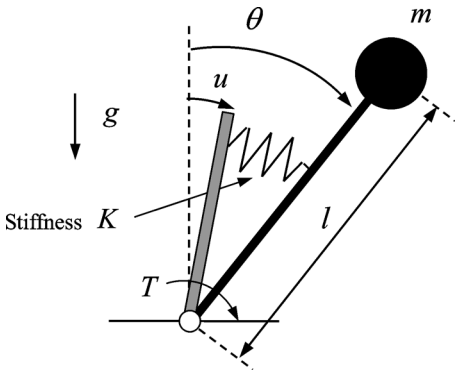

Figure 3. Simple inverted pendulum model with a compliant joint.

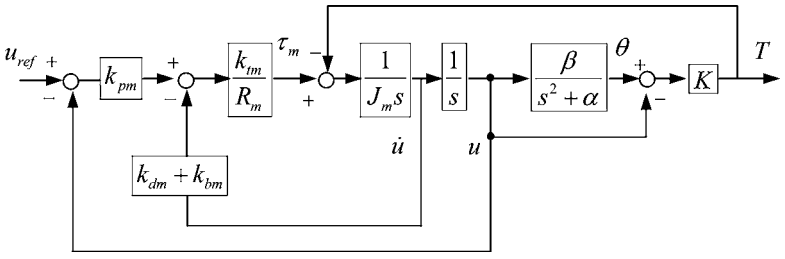

Figure 4. Transfer function from the reference position of an ankle to the torque output including the motor dynamics. k_{pm} is the proportional gain of position control, k_{bm} is the back-EMF constant, k_{dm} is the derivative gain of position control, k_{tm} is the torque constant, R_{m} is the terminal resistance, J_{m} is the inertia of an ankle axis and τ_{m} is the torque output of an ankle actuator.

3.2. Design of the damping controller

Even though the system is a lightly damped system, we can increase its damping ratio using the following feedback law as shown in Fig. 5:

$$u_{\text{ref}} = r - k_{\text{d}}\hat{\dot{\theta}}. \tag{5}$$

With this damping controller, we can reduce the oscillatory torque induced by the external force when the PD position control is applied at the ankle joint.

From (1), (2), (4) and (5), the following transfer function is derived:

$$\frac{\theta(s)}{r(s)} = \frac{K}{ml^2s^2 + k_{\text{d}}Ks + (K - mgl)} = \frac{\dfrac{K}{ml^2}}{s^2 + 2\xi\omega_{\text{n}}s + \omega_{\text{n}}^2}. \tag{6}$$

We can assign the damping ratio freely and the oscillatory motion can be suppressed effectively by changing k_{d} gain in the following equation:

$$k_{\text{d}} = 2\frac{\sqrt{ml^2(K - mgl)}}{K}\xi. \tag{7}$$

The stiffness is determined by the system characteristics. So, the stiffness should be identified by the experiment as described in Section 3.1. On the other hand, the damping controller adjusts the damping only, not the stiffness. The damping ratio can be assigned arbitrarily without changing the stiffness.

The steady-state value of the transfer function in (6) is:

$$\lim_{s\to 0}\frac{\theta(s)}{r(s)} = \frac{K}{K - mgl}, \tag{8}$$

and it is independent of k_{d} gain.

In (5), $\hat{\dot{\theta}}$ should be calculated from the following observer equation:

$$\dot{w} = -L_{\text{o}}w - \left(L_{\text{o}}^2 + \alpha\right)(y + Ku) + K\beta u, \tag{9}$$

$$\hat{\dot{\theta}} = \frac{1}{K}w + \frac{L_{\text{o}}}{K}(y + Ku), \tag{10}$$

where L_{o} is the observer pole.

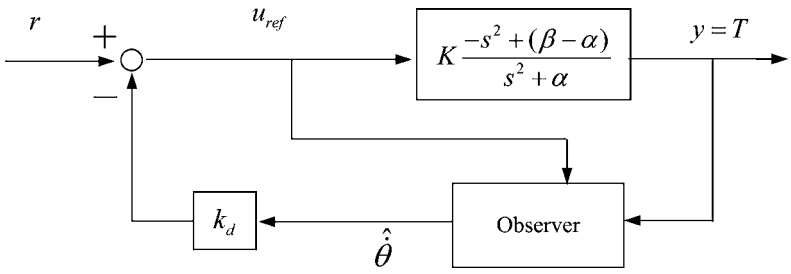

Figure 5. Block diagram of the damping controller.

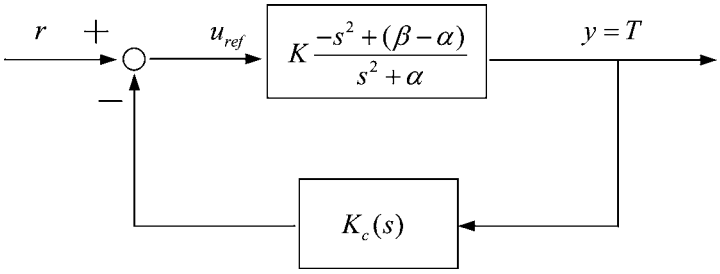

Figure 6. Block diagram of the practical damping controller.

For a practical implementation of the damping controller, the compensator transfer function in Fig. 6 is derived from (4), (5), (9) and (10).

$$K_{\mathrm{c}}(s) = p_{\mathrm{c}}\frac{s+p_{\mathrm{b}}}{s+p_{\mathrm{a}}}, \tag{11}$$

with:

$$p_{\mathrm{a}} = \frac{L_{\mathrm{o}} + (\beta-\alpha)k_{\mathrm{d}}}{1+k_{\mathrm{d}}L_{\mathrm{o}}},$$

$$p_{\mathrm{b}} = -\frac{\alpha}{L_{\mathrm{o}}},$$

$$p_{\mathrm{c}} = \frac{k_{\mathrm{d}}L_{\mathrm{o}}}{K(1+k_{\mathrm{d}}L_{\mathrm{o}})}.$$

Therefore, increasing the damping ratio in the light damped system can be regarded as making the simple first-order polynomial compensator that stabilizes the torque oscillation. The damping controller can be applied to the pitch and roll axes of the ankle with different stiffness.

3.3. Experimental verification of the damping controller

Figure 7 shows the experimental result of the proposed damping controller during the single support phase. When only PD control is applied to the ankle, it does not decay the oscillation caused from the external torque. However, with the damping controller, the oscillation decays out within 0.8 s. In the compensator, the assigned observer pole L_{o} is 6 rad/s and the damping ratio ξ is 0.707 where the stiffness of the system is 1033.4 Nm/s. This compensator works as a basic controller during the single support phase of biped walking. The effectiveness of the proposed controller is described in Section 5. The experimental results for the proposed damping controller can achieve stable walking.

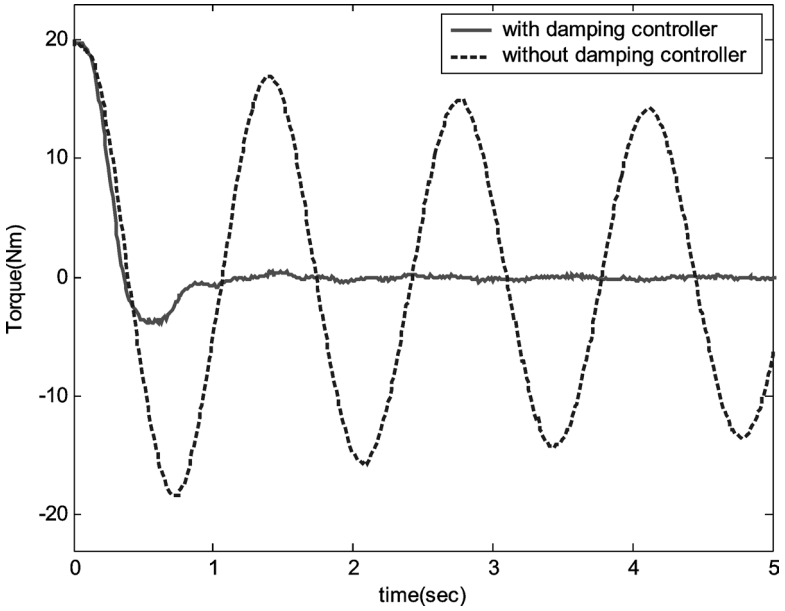

Figure 7. Time response of the measured torque (experimental result).

4. LANDING CONTROL

4.1. Landing orientation controller of the ankle joint

When a biped robot is walking by a prescribed walking pattern, the landing angle of the swing foot may be different from the prescribed landing angle. Moreover, the sole may not have perfect contact with the ground after landing. This can destabilize the robot. In the previous section, it was assumed that the sole is in perfect contact with the ground while the damping controller is applied. In order to enable perfect contact, a landing orientation controller is implemented before the damping controller is applied. The landing orientation controller is applied on the swing foot during landing and the damping controller is applied on the supporting foot after landing. It is known that a landing orientation controller can suppress instability and reduce impact [23]. From the viewpoint of the ankle position control, the essence of this landing orientation controller is somewhat different from the damping controller described in Section 3.2. The damping controller tries to maintain its position against the external force. However, the compliance of the required landing orientation controller should be soft enough that the position is easily shifted by the external force. In the landing orientation controller KHR-1, the ankle acts as the soft compliance that manages fast and stable ground contact without bouncing the foot off the ground. The reference angle of the ankle is controlled by the following equation in order to have the damping coefficient C_{L}

and stiffness K_L for a measured torque T:

$$u_{ref}(s) = r + \frac{T(s)}{C_L s + K_L}, \tag{12}$$

where the r is a reference angle of the ankle after solving the inverse kinematics. Tuning of C_L is performed by keeping K_L to zero, while creating a satisfying back drivability around the ankle pivot during the single support phase. By experiment, we selected C_L that makes the feedback system behave like a free-falling pendulum around the pivot during the single support phase. As a result, we tuned the C_L to 67 Nm·s/rad. K_L is used in order to prevent the divergence of the output angle, which is caused by the integration of the erroneous torque signal offset. In other words, K_L provides the leakage in the pure integrator. K_L was chosen as 200 Nm/rad in this experiment. If K_L becomes too large, the robot oscillates around the ankle pivot. As an alternative for preventing the divergence, we can also assign a dead zone at the torque input instead of using K_L.

4.2. Landing position controller

Prescribed walking patterns for the foot and the hip are shown in Figs 8 and 9. The coordinates X, Y and Z are the sagittal, frontal and vertical directions, respectively. During the single support phase, the position of the swing foot moves along the X- and Z-axis, and the position of the supporting foot is fixed on the ground. Landing of a swing foot makes the transition to the double support phase. During

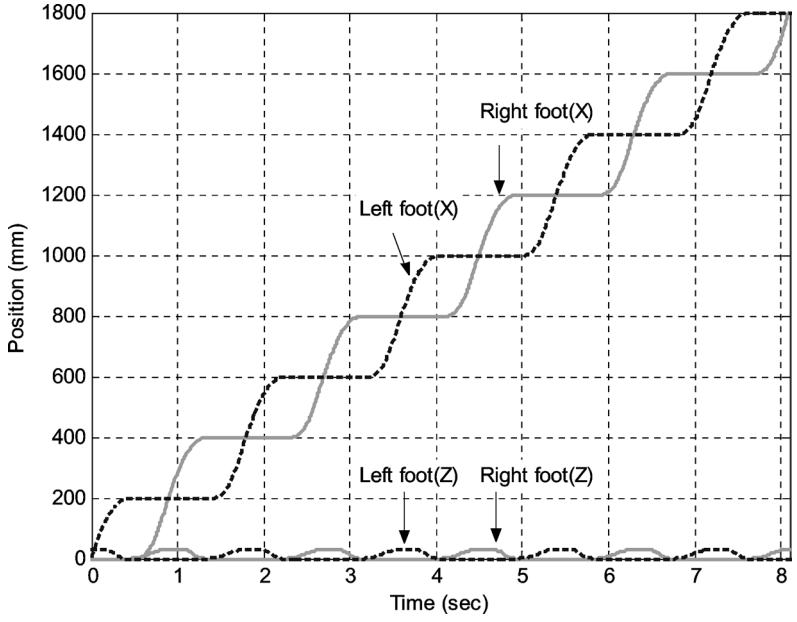

Figure 8. Prescribed trajectories of the foot position.

the double support phase, the position of both feet are fixed, but the hip position is free to move. The next transition to the single support phase occurs when the heel leaves the ground. The prescribed walking patterns are made up of these phases and transitions. However, the actual landing time of the foot may be different from the prescribed landing time when the robot walks on uneven terrain. When the actual landing occurs before the prescribed time, the use of the prescribed walking pattern without modification may cause undesirable effects. For example, if the position reference of the landing foot moves forward along the X-axis, the relative movement between the two feet will induce a vibration of the ankle during the next heel-off phase. In addition, the stretching of the landing foot along the Z-axis also causes a landing impact at that time. In order to solve these problems, a landing position controller is implemented to prevent the movement of the swing foot along the X- and Z-axis during unexpected landing [1]. Moreover, the landing position controller lengthens the stride on the next swing phase by the amount of loss and slowly stretches the foot after the landing is fully completed. By this modification of the feet position and recovery of the stride, the robot can walk stably at a given speed. When the swing foot touches the ground later than the desired contact time, the landing position controller is not used since it is not so effective in our experiment. Only when the actual landing occurs before the prescribed time is the position reference of the landing foot modified. In addition, it does not control the landing time and the time depends on the ground conditions. Our landing position controller needs the improvements mentioned above.

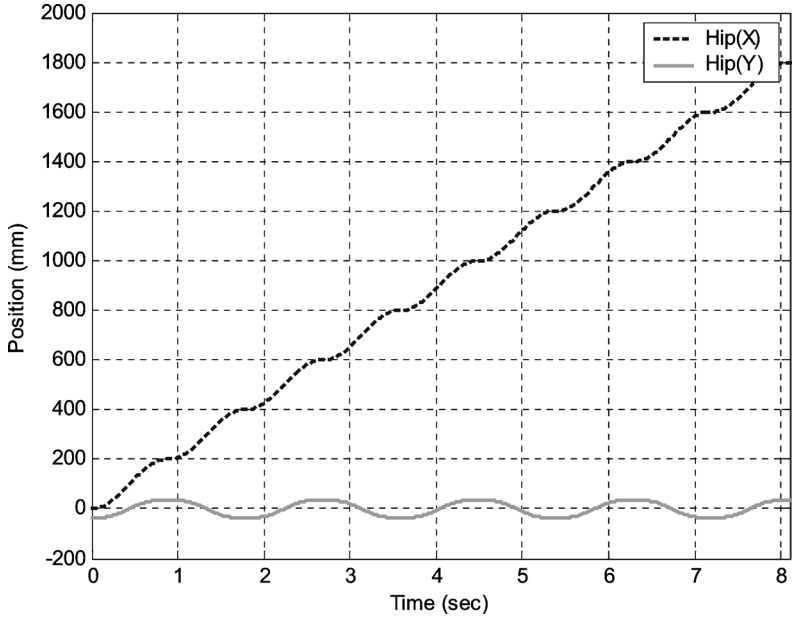

Figure 9. Prescribed trajectories of the hip position.

When the biped legs move, moments can be generated with the following conditions:

(i) When the landing time of the swing foot differs from the desired time, the landing impact can be applied as external moments.

(ii) When the inclination of the ground differs from the expected value.

(iii) When the moment is generated by an external force.

(iv) When the yaw moment of the robot cannot be neglected as the walking speed gets faster.

Our present control strategy does not actively generate the 3-d.o.f. motions of the upper body that compensates these moments, but it suppresses moments more or less for the above cases (i)–(iii). For example, in case (1), the landing position controller can reduce the external moment by absorbing the landing impact. In case (ii), the landing orientation controller reduces the external moment by achieving a soft contact with the ground during landing. This external moment occurs more significantly on irregular terrain. In this case, we should control it more actively using an inclination sensor. In case (iii), the damping controller suppresses the external moment by controlling the ankle position command with respect to the external force. In case (iv), the yaw moment should be compensated by controlling the yaw axis of torso in realtime, but it is not implemented yet in the control scheme of KHR-1.

5. OVERRALL CONTROL STRATEGY

In order to walk, walking patterns and an online controller are needed. In controlling KHR-1, three online controllers were implemented: the damping controller, landing orientation controller and landing position controller. The overall block diagram for dynamic walking control is shown in Fig. 10.

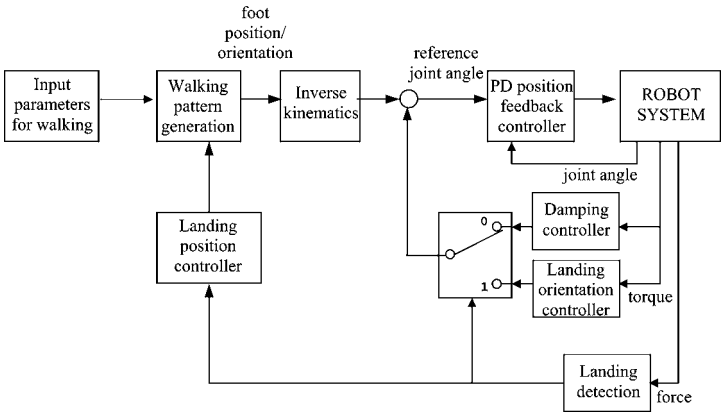

Figure 10. Block diagram of dynamic walking control.

Generally, foot trajectories and reference ZMP patterns are designed first in order to generate the walking pattern. Then, hip trajectories satisfying the reference ZMP can be calculated by lots of iterative methods by simulation. However, in our walking experiment, the exact solution for the walking pattern was not solved because the focus was on implementation of online controllers. Instead of designing the reference ZMP patterns, hip trajectories are simplified into functions for easy tuning in real experiments. The given foot trajectory contains some input parameters for walking. For example, step length l_{step}, step time t_{step}, maximum foot height and duty factor. Based on some information in foot trajectories, the hip trajectories are simplified into the following equations (see also Figs 11 and 12):

$$Y_{\text{hip}}(A_{Y\text{hip}}, t_{Y\text{delay}}) = \begin{cases} -A_{Y\text{hip}} & 0 \leqslant t < t_{Y\text{delay}} \\ -A_{Y\text{hip}} \cos\left(\dfrac{\pi(t - t_{Y\text{delay}})}{t_{\text{step}} - 2t_{Y\text{delay}}}\right) & t_{Y\text{delay}} \leqslant t < t_{\text{step}} - t_{Y\text{delay}} \\ A_{Y\text{hip}} & t_{\text{step}} - t_{Y\text{delay}} \leqslant t \leqslant t_{\text{step}}, \end{cases} \tag{13}$$

$$X_{\text{hip}}(t_{X\text{delay}}) = \begin{cases} \dfrac{l_{\text{step}}}{t_{\text{step}}} t - (t_{X\text{delay}} + 1)\left(\dfrac{l_{\text{step}}}{t_{\text{step}}} t - \dfrac{l_{\text{step}}}{2}\left\{1 - \cos\left(\dfrac{\pi}{t_{\text{step}}} t\right)\right\}\right) & \text{if } -1 \leqslant t_{X\text{delay}} \leqslant 0 \\ 0 \qquad\qquad 0 \leqslant t < t_{X\text{delay}} & \\ \begin{cases} \dfrac{l_{\text{step}}}{2}\left\{1 - \cos\left(\dfrac{\pi(t - t_{X\text{delay}})}{t_{\text{step}} - 2t_{X\text{delay}}}\right)\right\} & t_{X\text{delay}} \leqslant t < t_{\text{step}} - t_{X\text{delay}} \quad \text{if } 0 < t_{X\text{delay}} < \dfrac{t_{X\text{delay}}}{2} \\ l_{\text{step}} \qquad\qquad t_{\text{step}} - t_{X\text{delay}} \leqslant t \leqslant t_{\text{step}}. & \end{cases} & \end{cases} \tag{14}$$

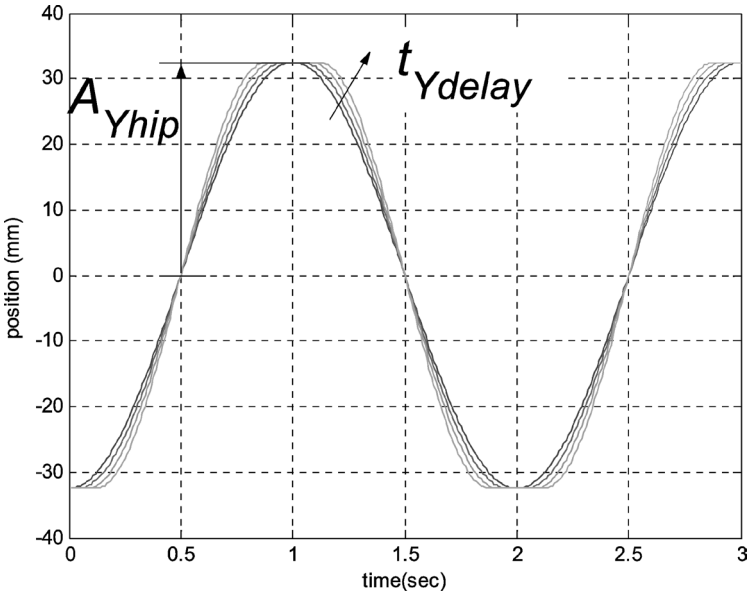

Figure 11. Hip trajectory Y_{hip} (lateral direction).

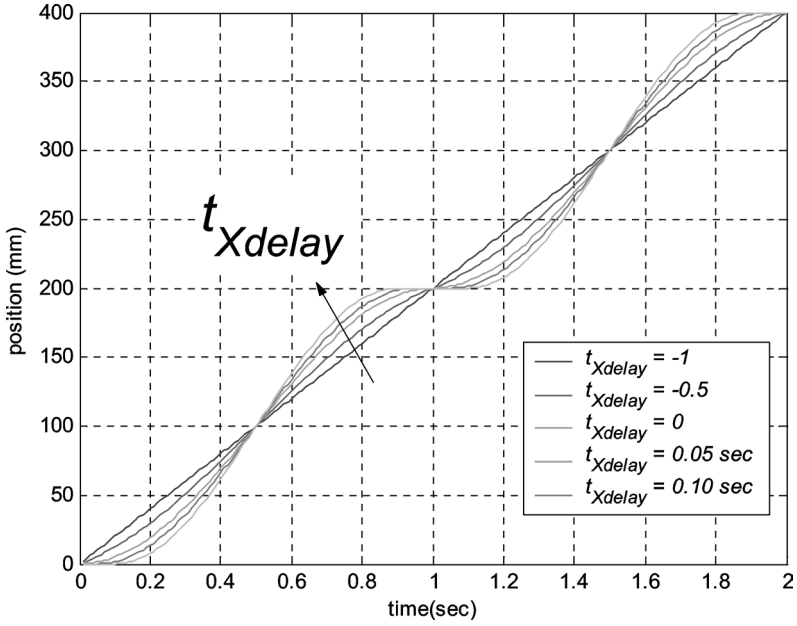

Figure 12. Hip trajectory X_{hip} (forward direction).

In this equation, $A_{Y\text{hip}}$, $t_{Y\text{delay}}$ and $t_{X\text{delay}}$ can change the shape of the hip trajectories, and they are also considered as tuning parameters for walking in our approach.

After walking patterns are generated, the relative feet positions and orientations are converted into reference joint angles. If the robot moves by PD position controller, torque and force is sensed. The damping controller is activated during the single support phase and the landing orientation controller is activated during the landing phase. By detecting force, two controllers are alternated. The landing orientation controller changes the foot angle to ensure perfect contact with the ground and the damping controller acts as a balance controller because the main cause of instability is lack of damping. When landing occurs before the expected time, prohibiting the movement of the landing foot increases the stability and reduces impact. The landing position controller is implemented for this purpose.

6. WALKING EXPERIMENT

In order to verify the performance of the proposed controller, a walking experiment was performed at steady state. The prescribed trajectories of foot and hip positions are shown in Figs 8 and 9, respectively. In Figs 8 and 9, the step length is 200 mm and the step period is 0.9 s. The hip height is kept at a constant height and the orientation of the sole is kept parallel to the floor. With the proposed controllers and the trajectories in Figs 8 and 9, stable walks could be achieved successfully.

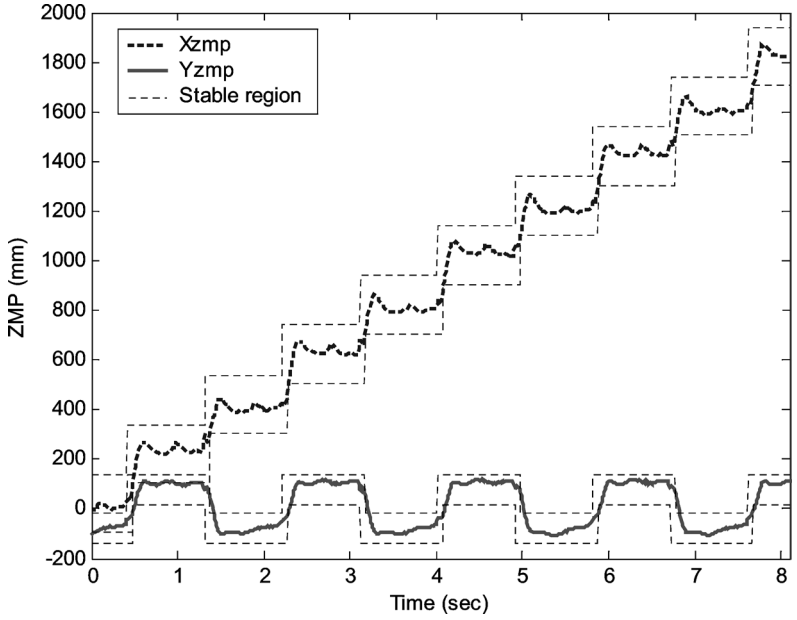

Figure 13. Measured ZMP.

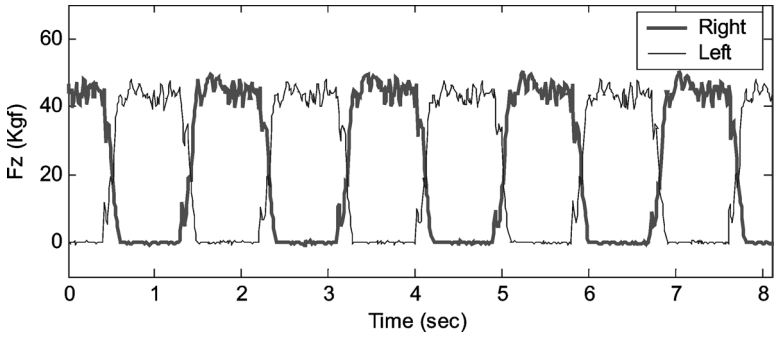

Figure 14. Measured force.

Figure 13 represents the experimental results (the measured ZMP is inside the stable region). In Fig. 14, measured normal forces are shifted periodically from one leg to the other. Figure 15 shows photographs of KHR-1 walking on a treadmill.

7. CONCLUSIONS

In this paper, we have described the method to realize dynamic walking for KHR-1 based on three controllers. The contributions of our paper are as follows:

(i) We noticed that the ZMP error occurred due to lack of damping when we performed position control during the single support phase. Thus, the simple inverted pendulum model with a compliant joint was proposed for the basis

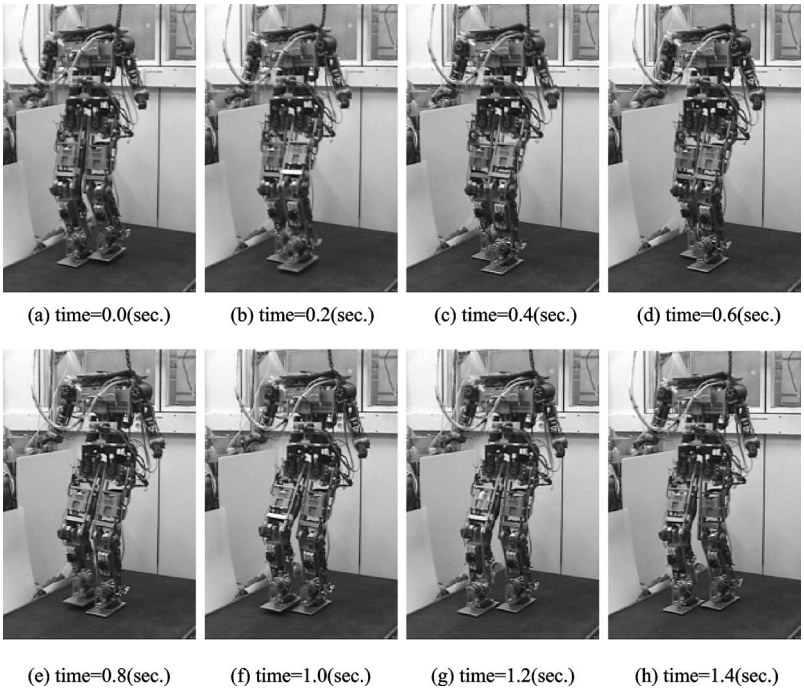

Figure 15. Photo sequence of the walking experiment.

of controller design to correct for the ZMP error. The proposed model has an advantage in easy parameter identification by experiment.

(ii) From this model, the damping controller was designed and its performance was evaluated by experiment. After the damping term was applied by the damping controller, the inherent oscillation was damped.

(iii) A landing orientation controller and a landing position controller were presented. These controllers were implemented to insure smooth and stable foot to ground interaction during landing.

(iv) The effectiveness of the whole control method was confirmed by the walking experiment.

At the time of writing of this paper, stable walking of 1 km/h could be realized with a step length of 250 mm and step period of 0.9 s. In order to increase the walking speed, optimized trajectory planning and the robust stabilization scheme using orientation sensor will be required.

Acknowledgements

This work was partly supported by the Korea Science and Engineering Foundation (KOSEF) through the Human-friendly Welfare Robot System Engineering Research Center at KAIST and Brain Korea 21 fund.

REFERENCES

1. K. Hirai, M. Hirose, Y. Haikawa and T. Takenaka, The development of honda humanoid robot, in: *Proc. Int. Conf. on Robotics and Automations*, Leuven, pp. 1321–1326 (1998).
2. K. Nishiwaki, T. Sugihara, S. Kagami, F. Kanehiro, M. Inaba and H. Inoue, Design and development of research platform for perception-action integration in humanoid Robot: H6, in: *Proc. Int. Conf. on Intelligent Robots and Systems*, Takamatsu, pp. 1559–1564 (2000).
3. Y. Sakagami, R. Watanabe, C. Aoyama, S. Matsunaga, N. Higaki and K. Fujimura, The intelligent ASIMO: System overview and integration, in: *Proc. Int. Conf. on Intelligent Robots and Systems*, Lausanne, pp. 2478–2483 (2002).
4. J. Yamaguchi, A. Takanishi and I. Kato, Development of a biped walking robot compensating for three-axis moment by trunk motion, in: *Proc. Int. Conf. on Intelligent Robots and Systems*, Yokohama, pp. 561–566 (1993).
5. Q. Huang, K. Yokoi, S. Kajita, K. Kaneko, H. Arai, N. Koyachi and K. Tanie, Planning walking patterns for a biped robot, *Trans. Robotics Automat.* **17**, 280–289 (2001).
6. K. Nagasaka, H. Inoue and M. Inaba, Dynamic walking pattern generation for a humanoid robot based on optimal gradient method, in: *Proc. Int. Conf. on Systems, Man, and Cybernetics*, Tokyo, pp. 908–913 (1999).
7. S. Kajita, F. Kanehiro, K. Kaneko, K. Fujiwara, K. Yokoi and H. Hirukawa, Biped walking pattern generation by a simple three-dimensional inverted pendulum model, *Advanced Robotics* **17**, 131–147 (2003).
8. H. O. Lim, Y. Yamamoto and A. Takanishi, Stabilization control for biped follow walking, *Advanced Robotics* **16**, 361–380 (2002).
9. K. Yokoi, F. Kanehiro, K. Kaneko, K. Fujiwara, S. Kajita and H. Hirukawa, A Honda humanoid robot controlled by AIST software, in: *Proc. Int. Conf. on Humanoid Robots*, Tokyo, pp. 259–264 (2001).
10. Napoleon, S. Nakaura, and M. Sampei, Balance control analysis of humanoid robot based on ZMP feedback control, in: *Proc. Int. Conf. on Intelligent Robots and Systems*, Lausanne, pp. 2437–2442 (2002).
11. M. Gienger, K. Löffler and F. Pfeiffer, Walking control of a biped robot based on inertial measurement, in: *Proc. of IARP Int. Workshop on Humanoid and Human Friendly Robotics*, Tsukuba, pp. 22–29 (2002).
12. K. Yokoi, F. Kanehiro, K. Kaneko, K. Fujiwara, S. Kajita and H. Hirukawa, Experimental study of biped locomotion of humanoid robot HRP-1S, in: *Experimental Robotics VIII*, B. Siciliano and P. Dario (Eds), pp. 75–84. Springer-Verlag, Berlin (2003).
13. S. Kajita, K. Yokoi, M. Saigo and K. Tanie, Balancing a humanoid robot using backdrive concerned torque control and direct angular momentum feedback, in: *Proc. Int. Conf. on Robotics and Automation*, Seoul, pp. 3376–3382 (2001).
14. S. Kagami, F. Kanehiro, Y. Tamiya, M. Inaba and H. Inoue, Autobalancer: an online dynamic balance compensation scheme for humanoid robots, in: *Proc. of 4th Int. Workshop on Algorithmic Foundations of Robotics*, Hanover, NH, pp. 329–340 (2000).
15. M. Vukobratovic, B. Borovac, D. Surla and D. Stokic, *Biped Locomotion: Dynamics, Stability, Control and Application*. Springer-Verlag, Berlin (1990).
16. T. Sugihara and Y. Nakamura, Whole-body cooperative balancing of humanoid robot using COG Jacobian, in: *Proc. Int. Conf. on Intelligent Robots and Systems*, Lausanne, pp. 2575–2580 (2002).
17. Q. Huang, K. Kaneko, K. Yokoi, S. Kajita, T. Kotoku, N. Koyachi, H. Arai, N. Imamura, K. Komoriya and K. Tanie, Balance control of a biped robot combining off-line pattern with real-time modification, in: *Proc. Int. Conf. on Robotics and Automation*, San Francisco, CA, pp. 3346–3352 (2000).

18. Napoleon, S. Nakaura and M. Sampei, Balance control analysis of humanoid robot based on ZMP feedback control, in: *Proc. Int. Conf. on Intelligent Robots and Systems*, Lausanne, pp. 2437–2442 (2002).
19. J. H. Kim, I. W. Park and J. H. Oh, Design of lower limbs for a humanoid biped robot, *Int. J. Human-friendly Welfare Robotic Syst.* **2**, 5–10 (2002).
20. J. H. Kim, S. W. Park, I. W. Park and J. H. Oh, Development of a humanoid biped walking robot platform KHR-1 — initial design and its performance evaluation, in: *Proc. of IARP Int. Workshop on Humanoid and Human Friendly Robotics*, Tsukuba, pp. 14–21 (2002).
21. J. E. Pratt, Exploiting Inherent robustness and natural dynamics in the control of bipedal walking robots, PhD Thesis, MIT, Cambridge, MA (2000).
22. J. H. Kim and J. H. Oh, Torque Feedback Control of the Humanoid Platform KHR-1, in: *Proc. of 3rd IEEE Int. Conf. on Humanoid Robots*, Karlsruhe and Munich, Germany (2003).
23. J. H. Park and H. Chung, Hybrid control for biped robots using impedance control and computed-torque control, in: *Proc. Int. Conf. on Robotics and Automation*, Detroit, MI, pp. 1365–1370 (1999).

ABOUT THE AUTHORS

Jung-Hoon Kim received the BS degree in Mechanical Design and Production Engineering from the University of Yonsei, Korea in 1997. He then received the MS and PhD degrees in Mechanical Engineering from Korea Advanced Institute of Science and Technology (KAIST), Daejeon, Korea, in 1999 and 2004, respectively. He is currently a Post-doctoral Fellow in the Department of Mechanical Engineering at KAIST. His research interests are in the areas of robotics, particularly the design and control of humanoid robots, autonomous systems, human–robot interaction, biomechanics, and sensors. He is a member of the KSME and ICASE.

Jun-Ho Oh received the BS and MS degrees in Mechanical Engineering from the University of Yonsei, Korea, and PhD degree in Mechanical Engineering from the University of Califonia, Berkeley, in 1977, 1979 and 1985, respectively. From 1979 to 1981, he was a Researcher with the Korea Atomic Energy Research Institute. Since 1985, he has been with the Department of Mechanical Engineering, KAIST, where he is currently a Professor. From 1996 to 1997, he was a Visiting Research Scientist in the University of Texas at Austin. His research interests include humanoid robots, adaptive control, intelligent control, nonlinear control, biomechanics, sensors and actuators. He is a member of the IEEE, KSME, KSPE and ICASE.